Constraints from rocks in the Taiwan orogen on crustal stress levels and rheology

Steven Kidder,[1,2] Jean-Philippe Avouac,[1] and Yu-Chang Chan[3]

Received 8 March 2012; revised 8 July 2012; accepted 10 August 2012; published 28 September 2012.

[1] Taiwan's Hsüehshan range experienced penetrative coaxial deformation within and near the brittle-plastic transition between ~6.5 and 3 Ma. This recent and short-lasting deformation in an active, well-studied orogen makes it an ideal natural laboratory for studying crustal rheology. Recrystallized grain size piezometry in quartz and Ti-in-quartz thermobarometry yield peak differential stresses of ~200 MPa at 250–300°C that taper off to ~80 MPa at ~350°C and ~14 MPa at ~400–500°C. Stress results do not vary with lithology: recrystallized quartz veins in slates and metasiltstones yield equivalent stresses as recrystallized grains in quartzites. A minimum strain rate of 2.9×10^{-15} s^{-1} associated with this deformation is calculated by dividing a strain measurement (axial strain ~0.3) in a strongly deformed quartzite by the available 3.5 m.y. deformation interval. We estimate a maximum strain rate of 7.0×10^{-14} s^{-1} by distributing the geodetic convergence rate throughout a region homogeneously deformed under horizontal compression. These stress, strain rate and temperature estimates are consistent with the predictions of widely applied dislocation creep flow laws for quartzite. The samples record stress levels at the brittle-plastic transition, indicating a coefficient of friction (μ) of 0.37 in the upper crust consistent with results based on critical taper. Integrated crustal strength of the Hsüehshan range amounts to 1.7×10^{12} N/m based on our analysis, consistent with potential energy constraints based on topography. Other strength profiles are considered, however high crustal stresses (>300 MPa) conflict with our analysis. The study supports the use of the recrystallized grain size piezometer in quartz as a quick and inexpensive method for resolving stress histories in greenschist facies rocks. For consistency with the independent constraints presented here, we find it accurate to within +20%/−40%, significantly better than previously recognized.

Citation: Kidder, S., J.-P. Avouac, and Y.-C. Chan (2012), Constraints from rocks in the Taiwan orogen on crustal stress levels and rheology, *J. Geophys. Res.*, *117*, B09408, doi:10.1029/2012JB009303.

1. Introduction

[2] Despite their importance in geodynamics and earthquake physics, the magnitude and distribution of stress in the lithosphere are poorly known and controversial [e.g., *Bürgmann and Dresen*, 2008; *Burov and Watts*, 2006; *Jackson*, 2002]. Quantifying differential stress (referred to below simply as "stress"), and developing and improving techniques for doing so [e.g., *Behr and Platt*, 2011], are thus important objectives in the Earth sciences. A promising tool for estimating paleostress in rocks is the recrystallized grain size piezometer, which is based on the inverse correlation between the size of grains formed during dislocation creep and stress [e.g., *Etheridge and Wilkie*, 1981; *Mercier et al.*, 1977; *Poirier*, 1985; *Twiss*, 1977]. Rapid and inexpensive measurements of grain size can be made in thin section, thus potential exists for routine use of the rock record to quantify stress histories. The usefulness of grain size piezometry, however, is limited by unknown inaccuracies introduced by extrapolation of laboratory-derived grain-size stress relationships to natural conditions [e.g., *Passchier and Trouw*, 2005].

[3] In this study we apply recrystallized grain size piezometry in an active and well-studied setting, Taiwan's Hsüehshan range (Figure 1), where results can be compared with independent constraints on stress levels [e.g., *Kaus et al.*, 2009; *Lacombe*, 2001; *Mouthereau and Petit*, 2003; *Suppe*, 2007]. We first document deformation conditions at middle-crustal levels, then catalogue available constraints on stress magnitude. We demonstrate that the recrystallized grain size piezometer in quartz is accurate to within the

[1]California Institute of Technology, Pasadena, California, USA.
[2]Now at Geology Department, University of Otago, Dunedin, New Zealand.
[3]Institute of Earth Sciences, Academia Sinica, Taipei, Taiwan.

Corresponding author: S. Kidder, Geology Department, University of Otago, PO Box 56, Dunedin 9054, New Zealand. (kidder@gps.caltech.edu)

0148-0227/12/2012JB009303

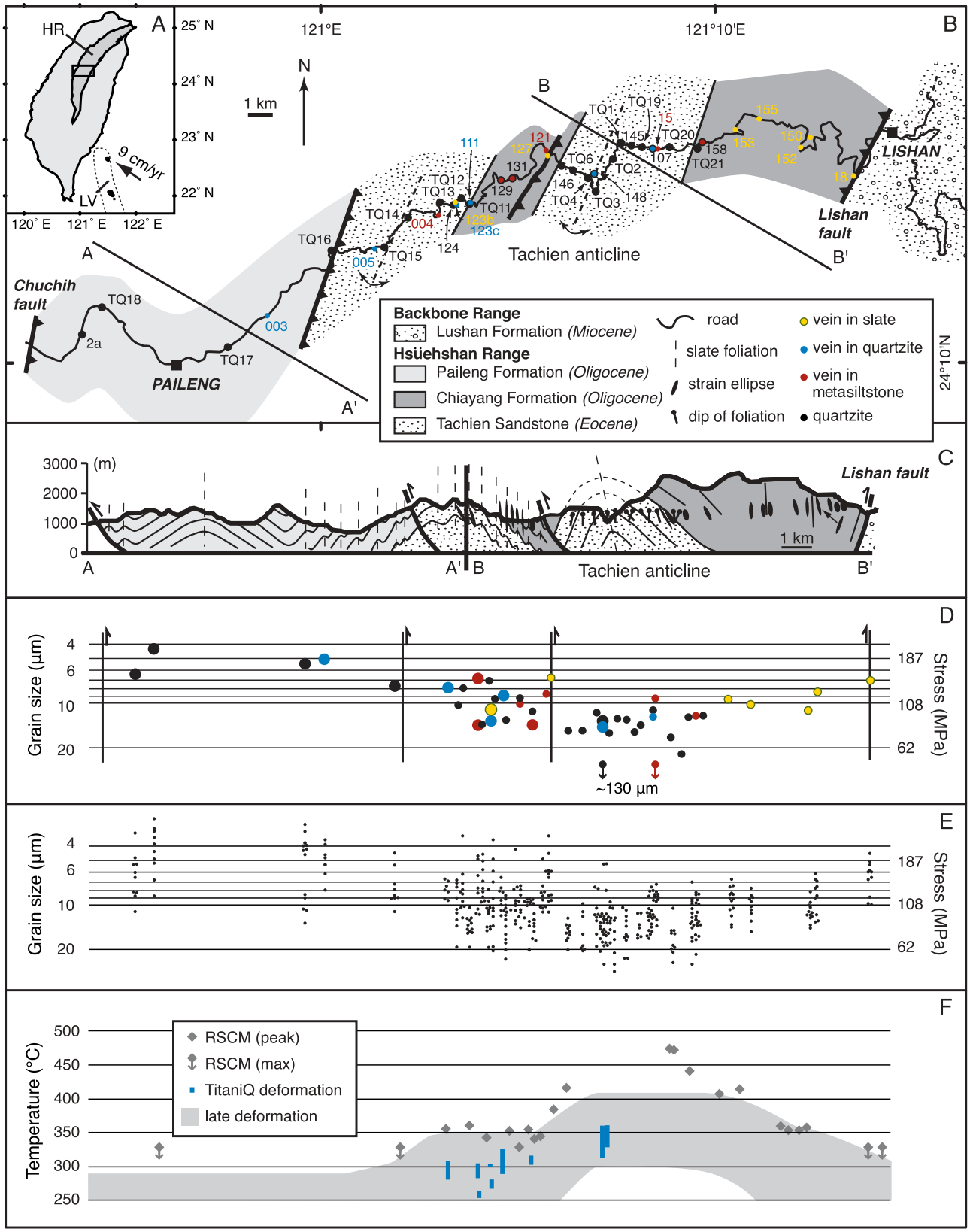
A
HR
LV
9 cm/yr
25° N
24° N
23° N
22° N
120° E
121° E
122° E
B
121°E
121°10'E
N
1 km
Tachien anticline
Lishan fault
LISHAN
Chuchih fault
PAILENG
TQ1
TQ2
TQ3
TQ4
TQ6
TQ11
TQ12
TQ13
TQ14
TQ15
TQ16
TQ17
TQ18
TQ19
TQ20
TQ21
2a
003
004
005
107
111
121
123b
123c
124
127
129
131
145
146
148
150
152
153
155
158
18
Backbone Range
Lushan Formation (Miocene)
Hsüehshan Range
Paileng Formation (Oligocene)
Chiayang Formation (Oligocene)
Tachien Sandstone (Eocene)
road
slate foliation
strain ellipse
dip of foliation
vein in slate
vein in quartzite
vein in metasiltstone
quartzite
24°10'N
C
3000
2000
1000
0
(m)
Lishan fault
1 km
D
Grain size (μm)
4
6
10
20
187
108
62
Stress (MPa)
~130 μm
E
F
Temperature (°C)
500
450
400
350
300
250
RSCM (peak)
RSCM (max)
TitaniQ deformation
late deformation

Figure 1

uncertainties of more widely applied techniques, and indicates a fairly weak middle crust in Taiwan.

2. Geologic Background and Deformation Conditions

[4] Taiwan is a result of the collision of the Luzon volcanic arc with the South China margin (Figure 1a). The rocks comprising the Hsüehshan range are late Tertiary passive margin quartzites and slates. Prior to collision they experienced only minor extensional deformation [*Clark et al.*, 1993; *Tillman et al.*, 1992]. Collision began at ~6.5 Ma at the latitude of the study area [*Lin et al.*, 2003], and ongoing exhumation in the Hsüehshan range exposes rocks deformed at depths up to ~20 km during early stages of collision [*Simoes et al.*, 2007]. Due to the obliquity of the collision, the orogen propagates southward at a rate of ~30–90 km/m.y. [*Simoes and Avouac*, 2006, and references therein]. While along-strike heterogeneities in the South China margin complicate the simple south-propagating model [e.g., *Byrne et al.*, 2011], modern-day southern Taiwan serves as a loose analogue for the study area during early collision.

[5] A strip map and cross section of the Hsüehshan range are shown in Figures 1b and 1c. The oldest unit in the stratigraphy is the Eocene-Oligocene Tachien "sandstone," a coarse-grained, massive quartzite with slate interbeds that contains 60–80% quartz (grains of quartz, quartzite, chert and quartz schist), detrital feldspar and mica, fragments of felsic volcanics and slate, and metamorphic chlorite and biotite [*Kidder et al.*, 2012]. The Tachien sandstone is overlain by the Oligocene Chiayang formation, consisting of slate and rare fine-grained quartzites, and the Paileng formation, an age-equivalent to the Chiayang formation comprising fine- to coarse-grained quartzite with minor slaty interbeds [*Ho*, 1988]. Precise ages of these units are uncertain due to lack of fossils. The structures shown in Figure 1 formed during collision as the passive-margin sedimentary cover was transferred from the down-going Eurasian plate to the Taiwan orogenic wedge. The deepest exposures occur in the core of the Tachien anticline, where early collisional deformation occurred within the biotite stability field, above ~400°C [*Kidder et al.*, 2012]. Deformation in most of the range—and significant retrograde deformation of the Tachien anticline [*Clark et al.*, 1993; *Kidder et al.*, 2012]—occurred at ~300°C (Figure 1f) [*Kidder et al.*, 2012]. We refer to this lower temperature deformation below as "late" deformation. *Kidder et al.* [2012] constrained deformation temperatures for late deformation using 1) Raman spectroscopy of carbonaceous material [*Beyssac et al.*, 2007], 2) the minimum temperature of ~250°C required for dynamic recrystallization in quartz [*Voll*, 1976; *Dresen et al.*, 1997; *Dunlap et al.*, 1997; *Stöckhert et al.*, 1999; *van Daalen et al.*, 1999], and 3) temperatures of vein emplacement and quartzite recrystallization using Ti-in-quartz thermobarometry [*Thomas et al.*, 2010]. Where possible, we use these Ti-in-quartz temperatures and associated errors below, but shift the temperatures +22°C to account for a small bias in the Ti-in-quartz results estimated by *Kidder et al.* [2012] for these rocks. *Kidder et al.* [2012] classified the late recrystallization within the "bulge" regime of *Stipp et al.* [2002, 2010], a rough analogue of the experimental dislocation creep "regime 1" of *Hirth and Tullis* [1992].

[6] Collisional deformation of the Hsüehshan range varies strongly from west to east. The Paileng formation, particularly in western portions, preserves sedimentary structures such as cross bedding and in many thin sections shows no perceptible strain. Limited penetrative deformation occurred by pressure solution creep (evidenced by occasional vertical cleavage striking NNE-SSW). Less than 1% of quartz in the Paileng formation is dynamically recrystallized, with recrystallization generally restricted to grain boundaries (e.g., Figure 2). These relatively undeformed quartzites contrast with those nearer the core of the Tachien anticline. Quartzite there is penetratively deformed (Figures 1c and 3a) with an axial strain of ~0.3 based on an R_f/ϕ analysis [*Chew*, 2003; *Lisle et al.*, 1983; *Ramsay*, 1967] of a representative sample (148d). This degree of strain is representative of quartzites in the inner 2–3 km of the anticline, with penetrative deformation decreasing moderately to the east and west. Based on the presence of strong undulose extinction, recrystallized grains and subgrains, and a weak lattice preferred orientation, much of this strain occurred by dislocation creep. A component of pressure solution creep cannot be excluded however, and in fact some finer-grained quartzites may have deformed exclusively by this mechanism as they show no recrystallization along grain boundaries and contain a solution cleavage. Minimum axial strains of ~0.2–0.7 [*Tillman and Byrne*, 1995] (see strain ellipses in Figure 1c) are evident in slates in the eastern and central Hsüehshan range indicating >30 km internal shortening [*Fisher et al.*, 2002].

[7] Quartz veins formed both during and prior to collision are common in the central Hsüehshan range [*Kidder et al.*, 2012; *Lu*, 1992; *Tillman et al.*, 1992; *Yen*, 1973]. Both types generally show evidence of some dynamic recrystallization

Figure 1. (a) Map of Taiwan showing the Hsüehshan range (HR), Luzon volcanic arc (LV), study area, and plate convergence vector [*Sella et al.*, 2002]. (b) Map of the study area showing sample localities and major structures. (c) Cross section modified from *Tillman and Byrne* [1995] showing major structures, strain ellipses in slate [*Tillman and Byrne*, 1995], and our foliation measurements in quartzite. (d) Average grain sizes and corresponding stress estimates plotted relative to position on cross section. Data points associated with good temperature constraints are enlarged. No systematic variation is evident between recrystallized grain size in quartzites and veins. (e) Individual line intercept measurements showing the fairly large spread of grain size from place to place within samples. (f) Summary of temperature constraints plotted relative to position on cross section. Raman spectroscopy of carbonaceous material (RSCM) serves as a peak temperature constraint; Ti-in-quartz temperature estimates [*Kidder et al.*, 2012] are deformation temperatures based on the Ti concentration of "late" recrystallized grains. The grey-shaded field summarizes deformation-temperature constraints for late deformation [*Kidder et al.*, 2012] including a minimum temperature of 250°C required for dynamic recrystallization. Comparison of Figures 1d and 1f shows a systematic increase in recrystallized grain size toward the warmer (more deeply exhumed) core of the range.

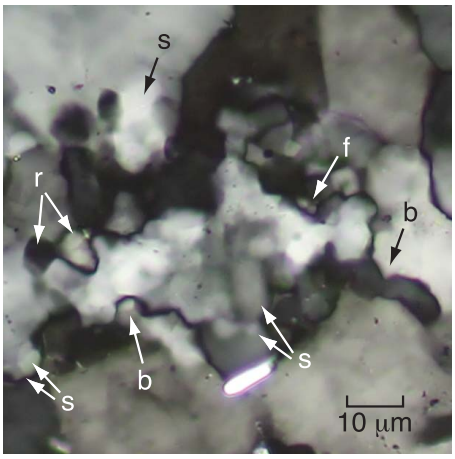

Figure 2. Cross-polarized microphotograph showing recrystallized grains "r," subgrains (or possible out-of-focus grains) "s," and grain boundary bulges "b" in a typical sample from the western Hsüehshan range (vein sample 003, deformation temperature 250–290°C). Recrystallization is incomplete and limited to a zone between larger grains. Extremely fine grains ("f," ~2 μm) are visible. Due to the thickness of the slide (~15 μm), linear intercepts drawn through this region necessarily approximate the true grain size since all grains and subgrains cannot be confidently resolved.

(e.g., Figure 2), indicating deformation at temperatures above 250°C (see above). Since collisional deformation occurred under generally retrograde conditions (for example early deformation occurred within the biotite stability field and late deformation did not [*Clark et al.*, 1993; *Kidder et al.*, 2012]), this observation indicates alternating brittle and plactic behavior (brittle behavior during vein formation, ductile deformation responsible for recrystallization, then further brittle deformation during exhumation). Some collisional veins can be shown to have undergone at least two brittle-plastic episodes, being plastically deformed, crosscut by new veins and then plastically deformed again [*Kidder et al.*, 2012]. Such behavior indicates some episodicity in strain rate, fluid pressure, or other deformation conditions [e.g., *Küster and Stöckhert*, 1998].

[8] The timing of deformation is constrained by collision at ~6.5 Ma and cooling of the core of the Tachien anticline through zircon fission track closure temperatures of ~200–260°C at ~3 Ma [*Liu et al.*, 2001]. Using 250°C as the cutoff temperature for dislocation creep in quartz, the fission track ages provide a minimum age for stresses based on recrystallized grain size. Dislocation microstructures, such as patches of recrystallized grains, are not generally overprinted by lower temperature features, suggesting that the 3 Ma cutoff age is a reasonable minimum estimate for the termination of shortening. Dividing the above strain estimate for the Tachien anticline by the 3.5 m.y. deformation interval yields a minimum estimate of strain rate of 2.9×10^{-15} s^{-1} for these rocks. We estimate a maximum strain rate of 7.0×10^{-14} s^{-1} by dividing the geodetic convergence rate by the width of the deformation zone. About 4.2 cm/yr convergence is accommodated west of the Eurasia-Philippine plate boundary [*Simoes and Avouac*, 2006]. Structural analyses by ourselves and *Tillman and Byrne* [1995] indicate penetrative deformation occurred over an ~19 km wide zone (Figure 1c). We cannot prove that penetrative deformation occurred simultaneously throughout this zone, however microstructures indicate fairly uniform coaxial deformation due to horizontal compression [*Fisher et al.*, 2002; *Tillman and Byrne*, 1995]. To accomplish this diachronously would require a propagating wave of shortening across the zone that is not indicated by the spatial distribution of (limited) thermochronologic data [*Liu et al.*, 2001; *Simoes et al.*, 2012].

[9] Deformation conditions were "wet" based on the presence of synkinematic biotite and chlorite [*Clark et al.*, 1993; *Kidder et al.*, 2012; *Yen*, 1973] and abundant fluid

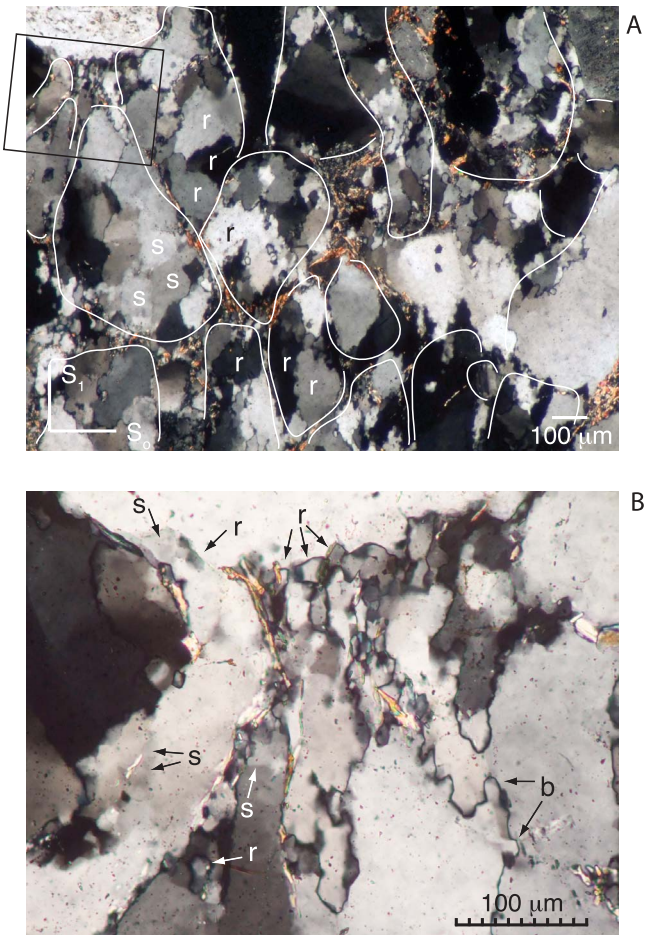

Figure 3. Cross-polarized microphotographs showing two phases of recrystallization in quartzite sample 148d. Photos are oriented perpendicular to bedding (S_o) and vertical foliation (S_1). (a) High temperature fabric formed during early deformation at deep structural levels. A similar recrystallized grain "r" and subgrain "s" size (~130 μm) and shape preferred orientation is shared by ~12 detrital grains (outlined in white) demonstrating that recrystallization post-dates deposition. Detrital grain outlines are based on the presence of micas and opaque material observed in plane polarized light. (b) Typical "late" dynamically recrystallized grains, subgrains, and grain boundary bulges "b" formed as deformation continued during exhumation and cooling. Late deformation of this sample occurred at a temperature of ~340°C. Inset in upper left of Figure 3a shows location of Figure 3b.

inclusions in veins and quartzites. Fluid inclusions in veins from the eastern edge of the Hsüehshan range are ~85 wt% H_2O [*Chan et al.*, 2005].

3. Methods

[10] Approximately 75 thin sections were made from quartzite and quartz veins in slates, metasiltstones, and quartzites collected in the Hsüehshan range. Measurements of recrystallized grain size were made in all samples containing recrystallized quartz. Grain size estimates were not made in quartzite samples containing veins in order to minimize potential effects of stress concentration associated with veining. Both collisional and precollisional veins were recrystallized during collision [*Tillman et al.*, 1992] and were lumped together in our analysis.

[11] Recrystallized grain size was measured under cross-polarized light using a linear intercept method [e.g., *Exner*, 1972] in thin (~30 μm) and ultrathin (~15 μm) sections. Geometric mean grain sizes and uncertainties are based on multiple linear intercepts of ~100 grains per sample (each linear intercept containing 5–25 grains), and are not the same as those that would be estimated by measuring each grain diameter individually [e.g., *Hacker et al.*, 1992]. Line intercepts were oriented and spaced on a case-by-case basis in order to intersect the maximum number of grains in recrystallized patches. Grain boundaries were defined as any visible sharp change in luminosity, thus optically visible subgrains were included in the analysis (e.g., Figures 2 and 3b). Subgrains were included because 1) the size of subgrains and recrystallized grains in our samples is similar enough to be indistinguishable by eye (e.g., Figures 2 and 3b), 2) recrystallization is spatially limited, such that patches of fully recrystallized grains are generally lacking, and 3) the ambiguity of distinguishing grains from subgrains is removed. Line intercepts were made "blindly," (i.e. without referring to structural position or earlier results) to minimize the potential for bias. No stereological correction was made.

[12] In samples where grain size is much smaller than the thin section thickness (e.g., Figure 2), the polarizing stage was rotated to help identify grains. Linear intercepts of such fine-grained areas may only approximate true grain size, however grains and subgrain structure at a scale as small as 2 μm are discernable (Figure 2) allowing for grain size estimates along some linear intercepts as small as ~3 μm (Figure 1e). Better precision measurements of the fine grains were not warranted given that uncertainty resulting from variation in grain size from place to place within samples (e.g., Figure 1e) is much greater than any plausible uncertainty introduced by the measurement technique.

[13] In (two) samples containing more than an order of magnitude variation in size between identifiable recrystallized fractions, the two fractions were measured separately as "fine" and "coarse" grains (e.g., Figure 3). Smaller variations in grain size between patches of recrystallized grains were assumed to result from a variation in internal stress field within samples and were averaged. In these cases we roughly weighted the distribution of linear intercept measurements according to the spatial distribution of different recrystallized fractions (i.e. if most recrystallization in a sample was of a particular grain size, most linear intercepts were taken through areas of that grain size).

[14] To avoid measuring recrystallization inherited from sedimentary sources, we first compared relatively undeformed quartzites from the western Hsüehshan range with the textures in more deformed samples. In most cases inherited recrystallization is easily avoided since the deformed quartzites are typified by relatively evenly distributed recrystallization, relatively uniform recrystallized grain size, and (in some cases) a shape-preferred orientation consistent with horizontal east–west compression (e.g., Figure 3a). Where ambiguous, recrystallization inherited from detrital sources was avoided by 1) restricting analyses to recrystallization concentrated along detrital grain boundaries or shared by 2–3 neighboring detrital grains, and/or 2) restricting analyses to recrystallized grains found in postdepositional quartz (e.g., quartz cement between detrital grains).

4. Stress Estimates

[15] The recrystallized grain size from late deformation ranges from ~4 to 22 μm (Table 1). These values are not likely influenced by post-deformational grain growth [e.g., *Hacker et al.*, 1992] since annealed textures [e.g., *Heilbronner and Tullis*, 2002] are not prevalent (Figures 2 and 3b), and the grain growth formulation of *Wightman et al.* [2006] predicts insufficient time for measurable growth since collision. Stresses corresponding to the measured grain size are ~210–57 MPa [*Stipp and Tullis*, 2003] and are plotted in Figure 1d for veins and quartzites (colored and black symbols, respectively). Some of the scatter in Figure 1d is due to deformation over a range of stress levels during cooling, as evident in Figures 4 and 5 where only data paired with well-constrained deformation temperatures are plotted. A grain size of ~130 μm (stress ~14 MPa) associated with the overprinted, early fabric (Figure 3a) in the Tachien anticline was estimated in two representative samples.

5. Discussion

5.1. Variability of Recrystallized Grain Size

[16] Recrystallized grain size and deformation temperature are grossly correlated in the Hsüehshan range (compare Figures 1d and 1f). Grain size and deformation temperature are greatest in the core of the Tachien anticline, and both decrease markedly to the west. The grain size data appear to cluster into three groups separated by the two main faults in the range, such that the deeper thrust sheets contain a progressively coarser recrystallized grain size. This trend demonstrates qualitatively that stress decreased with depth as expected in plastically deforming rocks [e.g., *Bürgmann and Dresen*, 2008].

[17] Due to the large sample size and the measurement of recrystallized grain size in a variety of rock types (quartzite; and veins in slate, metasiltstone, and quartzite), we can additionally address the effect on recrystallized grain size of stress concentrations due to viscosity contrast. It is unknown, for example, if veins in weak materials such as slate concentrate stress enough to significantly bias piezometric measurements in veins [e.g., *Kenis et al.*, 2005], or if grain-scale viscosity contrasts in polyphase rocks such as impure quartzite and granite cause significant variation in average stress in different minerals [e.g., *Bloomfield and Covey-Crump*, 1993]. The data presented in Figure 1d demonstrate

Table 1. Sample Locations, Grain Sizes, Stress Measurements, and Temperature Constraints

Sample	Type[a]	Easting[b]	Northing[b]	G.S.[c]	1σ	N	Stress[d]	+/−SE[e]	T (°C)[f]	SE[g]
002a	q	240222	2674693	6.4	2.3	104	153.5	4.4/4.2	<290	-
003	vq	247068	2675111	5.1	1.4	108	184.6	3.9/3.7	<290	-
4r2v2	vl	255063	2680085	6.8	1.5	102	145.7	2.6/2.5	258.8	2.5
4r345v2	vl	255063	2680085	14.1	3.4	101	81.9	1.6/1.5	294.3	6.7
005rp	vq	252309	2678535	7.9	1.0	115	130.0	1.3/1.2	293.8	5.4
15d	vl	264035	2682791	9.3	2.0	119	113.8	1.8/1.7	-	-
15dcrs	vl	264035	2682791	132.3	19.5	96	13.9	0.2/0.2	400–525	-
18c	vs	272472	2681848	7.0	3.1	117	142.1	4.8/4.4	-	-
107a	vq	263936	2682918	12.4	3.0	102	90.8	1.8/1.7	-	-
107b	q	263936	2682918	11.2	2.4	100	98.6	1.7/1.7	-	-
111br	vq	256048	2680584	8.9	1.8	102	118.0	1.9/1.8	274.3	3.4
121	vl	259460	2682666	8.7	1.9	108	120.3	2/1.9	-	-
123br	vs	255731	2680458	11.1	1.6	125	99.4	1/1	307.55	9.2
123cr	vq	255731	2680458	13.2	3.9	101	86.3	2/1.9	301.3	1.1
124f	q	255644	2680395	7.1	1.9	131	141.4	2.6/2.5	-	-
127b&c	vs	259507	2682469	6.8	2.3	140	146.9	3.4/3.2	-	-
129b	q	257529	2681538	9.3	2.7	104	114.3	2.6/2.5	-	-
129d	vl	257529	2681538	10.1	2.2	101	106.5	1.8/1.8	-	-
131b	q	258093	2681529	11.4	4.1	102	97.0	2.9/2.7	-	-
131gr	vl	258093	2681529	14.0	2.1	103	82.2	1/1	309.3	3.4
145	q	263352	2682879	15.7	4.2	109	75.2	1.6/1.5	-	-
146b	q	260673	2681855	15.4	4.4	107	76.5	1.7/1.6	-	-
148dr	q	261503	2681588	13.2	3.6	110	86.3	1.8/1.7	336.2	11.7
148dcrs	q	261503	2681588	128.2	27.2	109	14.2	0.2/0.2	400–550	-
148jr	vq	261503	2681588	14.5	5.5	115	80.1	2.3/2.2	344.2	8.0
150b	vs	270592	2683392	8.4	2.6	131	123.3	2.7/2.6	-	-
152b	vs	270167	2682977	11.2	1.7	109	98.2	1.1/1.1	-	-
153	vs	267395	2683616	9.4	2.2	100	112.7	2.2/2.1	-	-
155a&b	vs	268493	2684117	10.2	2.2	106	105.7	1.8/1.8	-	-
157b	q	265215	2682831	22.1	8.7	34	57.3	3.2/2.9	-	-
158b	q	265857	2683171	12.2	4.6	106	92.1	2.8/2.6	-	-
158b	vl	265857	2683171	12.2	2.7	104	91.8	1.6/1.6	-	-
TQ1	q	262746	2683033	13.0	3.5	106	87.6	1.9/1.8	-	-
TQ2	q	262327	2682370	12.8	2.8	111	88.6	1.5/1.4	-	-
TQ3	q	261709	2681214	15.9	6.5	105	74.3	2.4/2.3	-	-
TQ4	q	261397	2681612	11.6	3.9	103	95.6	2.6/2.4	-	-
TQ6	q	260122	2682121	15.4	2.2	102	76.5	0.9/0.9	-	-
TQ11	q	256407	2680543	13.0	4.4	110	87.2	2.3/2.2	-	-
TQ12	q	255907	2680623	9.4	5.5	103	113.2	5.5/4.9	-	-
TQ13	q	255085	2680460	14.0	2.2	113	82.6	1/1	-	-
TQ14	q	253739	2679923	7.9	2.5	104	129.1	3.2/3	-	-
TQ15	q	252606	2678618	10.3	4.0	103	104.9	3.3/3.1	-	-
TQ16	q	250654	2678560	7.7	2.0	106	132.6	2.8/2.6	<330	-
TQ17	q	246205	2674439	5.4	3.5	128	174.4	8.2/7.4	<290	-
TQ18	q	241051	2675978	4.3	1.9	100	209.8	7.6/7	<290	-
TQ19	q	263629	2682867	14.1	2.3	111	81.9	1/1	-	-
TQ20	q	264735	2682865	17.1	4.0	101	70.4	1.3/1.3	-	-
TQ21	q	265691	2682947	12.4	4.5	106	90.4	2.6/2.5	-	-

[a]Abbreviations: q, quartzite; vq, vein in quartzite; vl, vein in metasiltstone; vs, vein in slate.
[b]Taiwan grid, Hu-Tzu-Shan datum.
[c]Geometric mean grain size.
[d]Differential stress in MPa.
[e]Standard error of the mean.
[f]Temperatures reported with standard errors are Ti-in-quartz temperatures [*Thomas et al.*, 2010] from recrystallized collisional veins adjusted +22° based on the analysis of *Kidder et al.* [2012]. Other temperature constraints are discussed in the text.
[g]Standard error (excludes systematic error sources such as uncertainty in the geothermal gradient, [see *Kidder et al.*, 2012]).

that neighboring quartzites and veins have equivalent recrystallized grain sizes, and that the host lithology of veins does not strongly bias average recrystallized grain size. Veins in the likely weakest host phase, slate, show a reduction in grain size equivalent to stresses 0–20% higher than neighboring quartzites (the ambiguity results from a lack of quartzite in the easternmost portion of the range). Thus, while some stress concentration may have occurred, on average it did not result in differences that would significantly bias results.

5.2. Constraints on Middle Crustal Rheology

[18] It is often assumed, particularly in numerical models [e.g., *Kaus et al.*, 2008; *Yamato et al.*, 2009] that middle crustal rheology can be approximated using a flow law for dislocation creep of the form

$$\dot{\varepsilon} = A\sigma^{n}e^{(-Q/RT)} \quad (1)$$

where $\dot{\varepsilon}$ is strain rate, A is a material constant dependent on water fugacity, σ is differential stress (MPa) raised to an

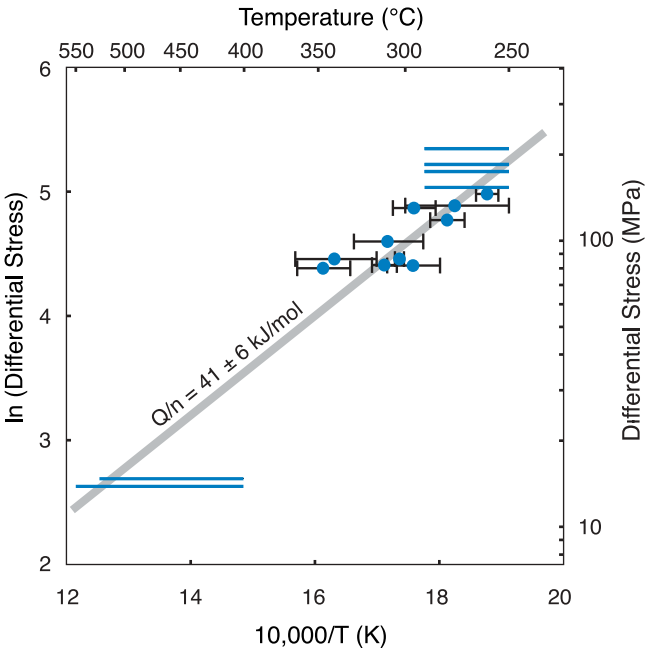

Figure 4. Arrhenius plot showing temperature and stress data for samples with well-constrained temperature. Data with error bars are Ti-in-quartz measurements. The ranges indicated in blue are for samples with minimum and maximum temperature constraints (low temperature samples from the western Hsüehshan range, and two high temperature samples from the Tachien anticline). Error bars on the vertical axis are negligible on this plot. The slope of the line through the data equals Q/nR if strain rate was relatively constant for the various samples (equation (2)). The Q/n value shown is consistent with dislocation creep flow laws for quartzite.

exponent n, Q is the creep activation energy (kJ mol^{-1}), R is the gas constant, and T is absolute temperature [e.g., *Poirier*, 1985]. Despite the heterogeneity of deformation mechanisms and rock types in the crust, assumed values of the parameters A, n and Q are generally based on experimental deformation of pure quartzite [e.g., *Kohlstedt et al.*, 1995]. This practice raises two important questions: Do quartzites in nature actually deform according to experimental predictions? If they do, can deformation of the crust—a heterogeneous suite of rocks containing little pure quartzite—be reasonably approximated using a quartzite flow law? Our dataset addresses these questions in two ways.

[19] We first calculate the viscosity of quartzite in the Hsüehshan range using our estimates of stress and strain rate, and compare it to the viscosity predicted using commonly applied quartzite flow laws. This procedure is done for the two representative samples from the Tachien anticline core, since this is the only region where reasonably accurate strain measurements in quartzites were possible. Both samples contain a remnant early set of coarse recrystallized grains that are overprinted by finer recrystallized grains (Figure 3). Deformation temperature is better constrained for the late, high stress deformation at ~330°C (Figure 1f), and we calculate a viscosity for these conditions between 7.4×10^{20} and 3.6×10^{22} Pa s. During early deformation at ~400–500°C, we calculate a viscosity between 1.2×10^{20} and 5.8×10^{21} Pa s. (These ranges in viscosity include an estimated uncertainty in the stress measurements of +20%/−40%, see below.) These viscosities are consistent with those predicted by the widely used quartzite flow laws of *Paterson and Luan* [1990] and *Hirth et al.* [2001] assuming a water fugacity from *Pitzer and Sterner* [1994] (with help from Wither's fugacity calculator, http://www.geo.umn.edu/people/researchers/withe012/fugacity.htm) and hydrostatic fluid pressure (see below). The consistency between our measurements and the flow law predictions can be seen graphically in Figure 5, where these data are plotted as four larger black dots. The shaded areas in Figure 5 representing the two flow laws indicate the range of predicted stresses given our strain rate constraints. At a minimum, this result demonstrates a consistency under natural conditions between the two independent approaches: recrystallized grain size piezometry and experimentally derived flow laws. It also strengthens the case that these flow laws accurately predict the rheology of real quartzite under geologic conditions (at least at temperatures of 300–500°C), despite the impurity (20–40% non-quartz phases) of the quartzite.

[20] Our data also allow a test of the applicability of such flow laws to a middle crust formed only partially of quartzite and deformed only partly by dislocation creep since: 1) roughly a third of the Hsüehshan range (the Chiayang formation) is composed of slate with a strong pressure solution cleavage, 2) slate interbeds and fine grained quartzites deformed by pressure solution are also common in the Paileng and Tachien quartzites, and 3) the dynamic recrystallization of collisional veins indicates brittle processes at elevated temperatures. Assuming a flow law of the form given in equation (1), the ratio of the parameters Q and n associated with this multi-mechanism, multi-lithology deformation can be constrained using our stress-temperature data. We reformulate equation (1) as

$$\ln(\sigma) = \mathrm{B} + \mathrm{Q}/(\mathrm{nRT}) \qquad (2)$$

where B incorporates A, n and $\dot{\varepsilon}$. The slope on an Arrhenius plot of $\ln(\sigma)$ vs. 1/T is Q/nR (Figure 4). We assume here that bulk strain rates for the different exposed crustal levels were equal. Since the Hsüehshan range is a pop-up structure characterized by coaxial strain [*Clark et al.*, 1993], it seems likely that shortening rates would not be dramatically different between the different crustal levels. We find a slope equivalent to a value for Q/n of 41 ± 6 kJ/mol (95% confidence) using the "model 2" linear regression of *Ludwig* [2001]. This value is consistent with the Q/n values of the quartzite flow laws of *Hirth et al.* [2001] and *Paterson and Luan* [1990]. While this agreement may add some support to the practice of using such flow laws in numerical models of the crust, the result is non-unique. For example, Q/n values estimated for pressure solution creep (n = 1) range from 15 to 113 [e.g., *Kawabata et al.*, 2009]. The ability, demonstrated here, to estimate Q/n without relying on high-temperature laboratory experiments is a useful approach to better constrain rock rheology, and would be particularly powerful if used in combination with independent constraints on n [e.g., *Grigull et al.*, 2012; *Kenis et al.*, 2005; *Lan and Hudleston*, 1995; *Treagus and Treagus*, 2002].

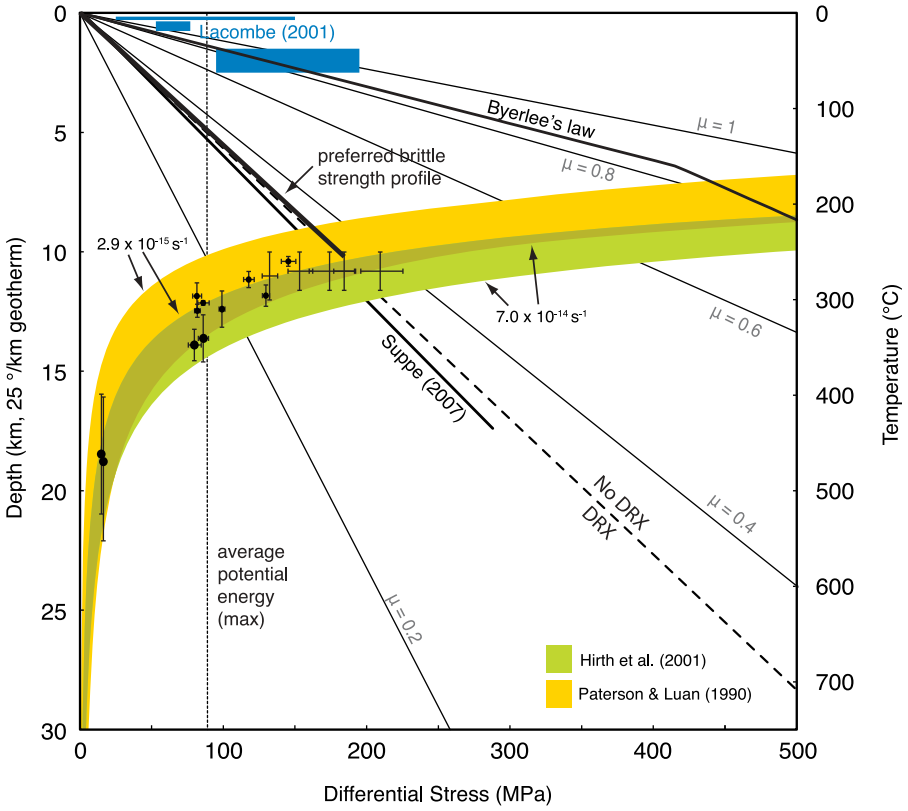

Figure 5. Stress–depth diagram demonstrating agreement between temperature-stress results and independent constraints: maximum stress estimates provided by Byerlee's law, calcite twinning [*Lacombe*, 2001] and Goetze's criterion (dashed line); maximum potential energy based on topography (dotted line); Taiwan coefficient of friction (μ) from *Suppe* [2007]; and predictions of widely used flow laws [*Hirth et al.*, 2001; *Paterson and Luan*, 1990] assuming strain rates estimated for the Hsüehshan range (the four larger black dots are data from the Tachien anticline where the strain measurement was made and are therefore most directly comparable to the flow laws). Data and constraints are plotted assuming a 25°/km geotherm and hydrostatic fluid pressure (see text). Black dots are Ti-in-quartz temperature estimates with 2σ standard errors. Error bars without symbols represent data with only minimum and maximum temperature constraints: high stress data use a minimum temperature estimate of 250°C required for dynamic recrystallization in quartz and a maximum temperature of 290–300°C based on stratigraphic constraints and unpublished Raman spectroscopic data for carbonaceous material (RSCM) (O. Beyssac, personal communication). The two low-stress data use an RSCM peak temperature constraint and a minimum constraint of 400°C [*Kidder et al.*, 2012].

5.3. Strength of the Taiwan Orogenic Wedge

[21] As a first approach, lithospheric strength can be considered a function of the two best-understood deformation mechanisms in rocks: Mohr-Coulomb friction and dislocation creep [e.g., *Scholz*, 2002]. At cold temperatures where friction dominates, strength increases linearly with effective confining pressure. As temperature increases with depth, dislocation creep accommodates increasing amounts of imposed strain and strength decreases. The crust is strongest where similar stresses are required to activate each process, the "brittle-plastic transition." While deformation mechanisms such as pressure solution and semibrittle flow may in reality act to blunt peak stresses predicted by the two-mechanism approach [e.g., *Kohlstedt et al.*, 1995], dislocation creep and resulting dynamic recrystallization of quartz at the brittle-plastic transition are both expected and observed [e.g., *Küster and Stöckhert*, 1998]. It is thus likely that the highest stresses in the crust are recorded in quartz dynamically recrystallized at the brittle-plastic transition.

[22] There are several lines of evidence suggesting that our higher stress samples were deformed within the brittle-plastic transition: 1) The depth distribution of earthquakes in southern Taiwan (the present-day analogue to our study area) shows a clear peak at ~10 km (e.g., *Mouthereau and Petit* [2003] using data from the Central Weather Bureau Seismic Network [*Shin*, 1992]). Recrystallization of Hsüehshan range quartzites occurred roughly at this depth level and lower assuming a geothermal gradient of 25°/km (Figure 5). (Geotherm estimates for central Taiwan vary, however this estimate is consistent with the 25–30°/km gradient in Raman spectroscopy of carbonaceous material (RSCM) temperature with stratigraphic depth in the study area [*Beyssac et al.*, 2007], the thermal history modeled by *Simoes et al.* [2007], and the average thermal gradient in exploration wells in Taiwan [*Zhou et al.*, 2003]). 2) Overlapping brittle and

plastic deformation evident in veins from the central Hsüehshan range typifies behavior expected at the brittle-plastic transition. 3) The highest stress samples come from the western part of the Hsüehshan range, where penetrative deformation was minimal. Shortening here apparently was accomplished primarily via faulting, which in comparison with the penetratively deformed central Hsüehshan range suggests deformation conditions near the shallowest depths of the brittle-plastic transition. 4) Based on Taiwan wedge tapers, *Carena et al.* [2002] estimated that the brittle-plastic transition occurs at a depth of 15–20 km (within the estimated depth range of our samples).

[23] Assuming that our lowest temperature and highest stress data reflect conditions at the brittle-plastic transition, we follow *Behr and Platt* [2011] in constructing a crustal strength envelope by fitting a line from the surface to a value typical of our highest stress samples, ~200 MPa (Figure 5, preferred brittle strength profile). The coefficient of friction μ implied by this profile is ~0.37 assuming hydrostatic fluid pressure. We assume hydrostatic fluid pressure since effective pressure ($P_{lithostatic} - P_{fluid}$) must be greater than differential stress in order for dislocation creep and dynamic recrystallization to occur ("Goetze's criterion") [*Kohlstedt et al.*, 1995]. Under hydrostatic conditions, effective pressure (dashed line in Figure 5) falls very close to the highest stress data, thus ruling out higher fluid pressure at the brittle-plastic transition. This rationale led to similar conclusions by *Küster and Stöckhert* [1998] and *Behr and Platt* [2011].

[24] Further insights into crustal strength in Taiwan can be gained by comparison with independent estimates of stress levels in Taiwan. Based on critical taper theory *Suppe* [2007] found that stress (σ_D) in Taiwan increases with depth in the brittle crust according to the relationship $\sigma_D = W\rho gz$, where W = 0.6. This constraint nearly coincides with the brittle portion of our preferred strength envelope (Figure 5). Calcite twin orientations in southern Taiwan [*Lacombe*, 2001] provide an additional "order of magnitude" constraint on stress levels (Figure 5). Finally maximum strength can be estimated based on Coulomb frictional-failure theory and the experimental results of *Byerlee* [1978] assuming hydrostatic fluid pressure

$$\tau = \mu\sigma_{eff} \quad \sigma_n < 200\,\text{MPa} \tag{3a}$$

$$\tau = 50 + \mu\sigma_{eff} \quad 200\,\text{Mpa} < \sigma_n < 1700\,\text{MPa} \tag{3b}$$

where τ is shear stress in MPa, μ is the friction coefficient, and σ_{eff} is effective confining pressure in MPa. *Byerlee* [1978] found values of μ = 0.85 and 0.6 for equations (3a) and (3b), respectively (i.e. "Byerlee's law"). Stress levels in boreholes reaching depths of 3–8 km in Europe and Western North America are consistent with *Byerlee*'s [1978] results, fitting equation (3a) well with μ = 0.6–1 [*Townend and Zoback*, 2000]. The strength envelope labeled "Byerlee's law" in Figure 5 is a maximum constraint since fluid pressure in shallow wells in Taiwan often exceeds hydrostatic [*Suppe and Wittke*, 1977; *Yue*, 2007]. We suggest that the calcite twin study of *Lacombe* [2001] also overestimates stress since two of the three data points indicate higher stresses than Byerlee's law. It is unclear why *Suppe*'s [2007] and our μ are lower than global borehole estimates. Perhaps there is a fundamental difference in crustal strength between the generally cratonic study areas probed by the boreholes and the low-grade metasedimentary rocks comprising much of the Taiwan orogenic wedge.

[25] These constraints on brittle strength can be combined with a curve fit through our stress-temperature data to constrain integrated crustal strength (Figure 6). As a weak brittle endmember we use our preferred μ of 0.36 (Figure 6a). As a strong endmember we construct a strength envelope assuming Byerlee's law (Figure 6b). Integrating these strength envelopes to a depth of 30 km yields total crustal strengths of 1.7×10^{12} N/m and 3.9×10^{12} N/m, respectively. These values can be compared with the horizontal stress required to support topography assuming isostatic balance and no contribution from vertical stresses (e.g., flexure). The Hsüehshan range rises to an altitude of ~2.5 km in the long-wavelength topography with a Moho depth of 35–45 km beneath the range and 29–37 km in western Taiwan [*Kim et al.*, 2004; *McIntosh et al.*, 2005; *Shih et al.*, 1998; *Ustaszewski et al.*, 2012]. Following *Molnar and Lyon-Caen* [1988], we calculate a potential energy difference of 2.7×10^{12} N/m, equivalent to a strength of ~90 MPa averaged over a 30 km thickness (Figures 5 and 6). Since we ignore vertical stress contributions to topographic support, this calculation provides an upper limit on crustal strength in Taiwan. The "preferred" profile (Figure 6a) is consistent with this constraint, while the higher strength end member (Figure 6b) is overly strong. Thus the high strength derived from Byerlee's law would only be consistent with the potential energy constraint if the crustal strength estimate is truncated [e.g., *Kohlstedt et al.*, 1995] at a stress of ~240 MPa or smaller (Figure 6c). Intermediate values for the coefficient of friction (μ = 0.36–0.65) would not require truncation and potentially permit a maximum stress up to ~300 MPa. This scenario however is less consistent with other constraints mentioned above. In any case, the low stresses required by this analysis conflict with the high stresses (>400 MPa) suggested by *Mouthereau and Petit* [2003] and considered by *Kaus et al.* [2009].

[26] While we find peak stresses at ~12 km similar to those estimated by *Suppe* [2007], the data on which his critical taper estimate is based were interpreted to indicate a brittle wedge to depths of 15–20 km [*Carena et al.*, 2002]. The crustal strength profiles plotted in Figures 5, 6a, 6b, and 6c suggest a much weaker crust at depths of 10–20 km. This discrepancy could be rectified by reducing our assumed geothermal gradient to 18°/km (or smaller), a low value but within the range of existing estimates in central Taiwan [e.g., *Gourley et al.*, 2007]. This possibility is plotted in Figure 6d. Given the potential energy constraint, this scenario also requires μ = ~0.36 (or lower). The consistency of such a low geotherm with thermochronologic and metamorphic data can be tested in future studies.

5.4. Accuracy of the Recrystallized Grain size Piezometer in Quartz

[27] The overall consistency of our results with independent experimental and theoretical constraints on stress levels is striking (Figure 5). Stresses are consistent with the predictions of the most widely applied quartzite flow laws. The coefficient of friction we estimate based on peak stress measurements is nearly identical to that predicted by critical

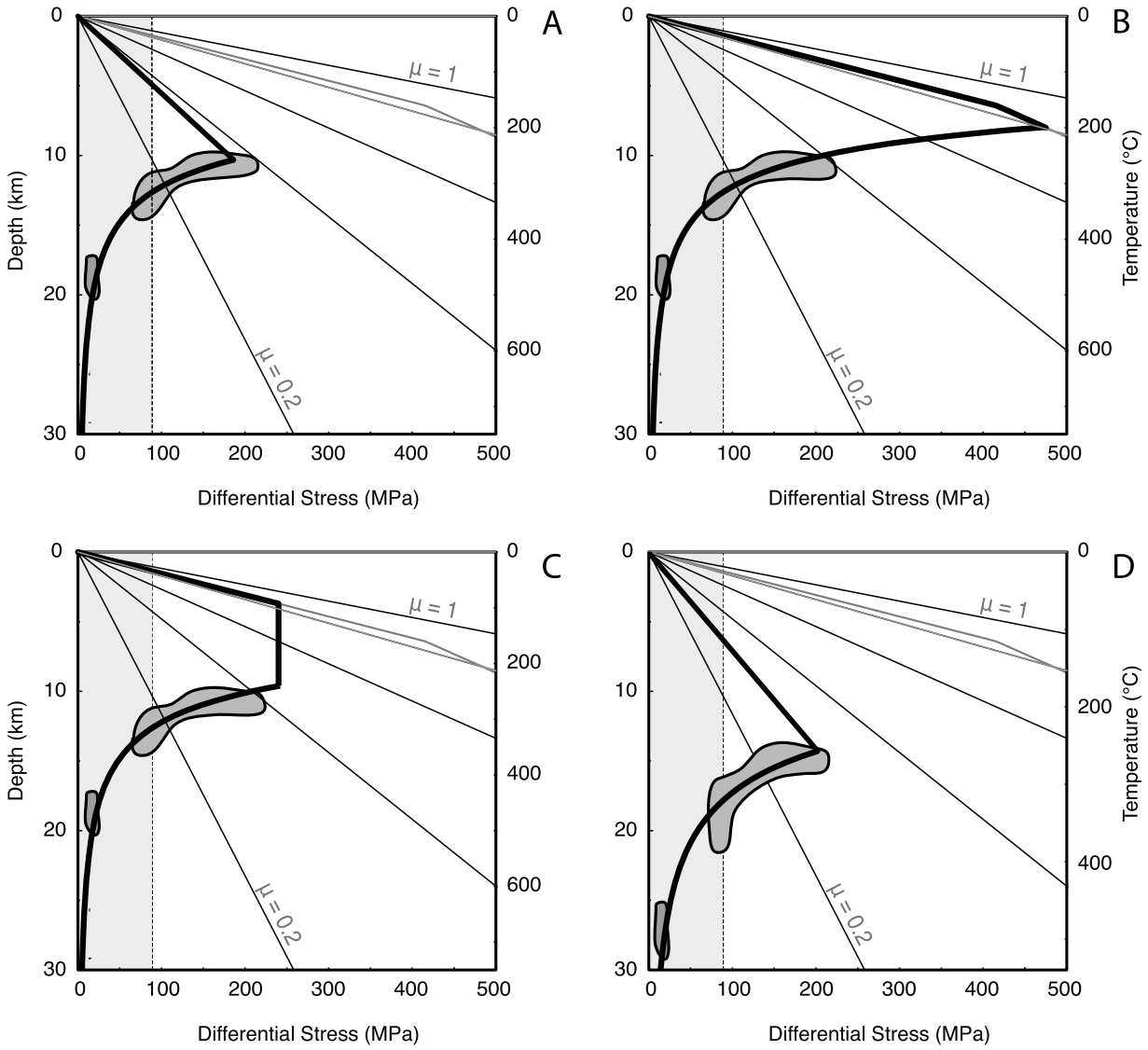

Figure 6. Alternative strength profile scenarios (thick dark lines) demonstrating that peak long-term stress in the Hsüehshan range is below ~300 MPa. To satisfy the potential energy constraint, the area defined by the strength profiles must be less than the area of the light grey box. Paleopiezometric data fields (dark grey), Byerlee's law (kinked black line), and reference values for friction coefficient μ (thin lines) are also shown. The curved portion of the strength profiles is a fit through the paleopiezometric data (using *Hirth et al.* [2001] with strain rate 2×10^{-14} s^{-1}, and f_{H2O} = 37 MPa). (a) Preferred strength profile assuming that peak stresses in recrystallized quartz represent peak crustal stresses. (b) Strength profile based on Byerlee's law (exceeds the maximum potential energy constraint). (c) Same profile as in Figure 6b, but truncated at a stress of 240 MPa to satisfy the potential energy constraint. (d) Strength profile constructed as in Figure 6a, but assuming a geothermal gradient of 18°/km. Brittle portion corresponds to μ = 0.3, the potential energy constraint limits μ to 0.37 or smaller.

taper theory [*Suppe*, 2007]. Stress estimates fall below maximum constraints provided by Byerlee's law and *Lacombe*'s [2001] calcite twinning study. Our data are generally consistent with Goetze's criterion ($\sigma_D < P_{eff}$ for plastic flow). Simple crustal strength profiles based on the data (Figures 6a, 6c, and 6d) satisfy potential energy constraints from topography. This comparison provides the strongest evidence to date that the laboratory-based stress-grain size relationship for quartz is accurate under natural conditions (at least at low temperatures). The relationship holds in the Hsüehshan range despite the presence of fluids and competing deformation processes.

[28] To our knowledge, the only existing estimate of the accuracy of the recrystallized grain size is an "order of magnitude" [*Stöckhert et al.*, 1999]. The piezometer is clearly outperforming this evaluation in the Hsüehshan range. To maintain consistency with the various independent constraints provided here, we estimate the *Stipp and Tullis* [2003] piezometer to be accurate to within +20%/−40%. An overestimate of 20% places our data at higher stress

values than predicted by the quartzite flow laws, and would violate Goetze's criterion. An underestimate by 40% places peak stresses significantly (50 MPa) below the stress level estimated by *Suppe* [2007] at 12 km depth, and would be even more discrepant with Byerlee's law and global borehole estimates.

[29] This constraint on the accuracy of the *Stipp and Tullis* [2003] piezometer is at odds with a recent alternative recrystallized grain size–stress relationship, the "paleowattmeter" of *Austin and Evans* [2007, 2009]. The paleowattmeter generally provides a good fit to laboratory data, however it predicts a temperature dependence that results in very low stress estimates for geologic conditions (e.g., ~1 MPa for the late deformation in sample 148d). Stresses this low are ruled out by the above analysis. This discrepancy does not necessarily indicate a flaw with the paleowattmeter formulation, which is heavily dependent on parameters whose values are not well known. The temperature dependence stems from the difference in activation energy for grain growth and dislocation creep, and it may be that an improved understanding of grain growth rates in quartz would lead to better results.

5.5. Is Steady State a Prerequisite for Piezometry?

[30] Despite the difficulty of demonstrating that a rock has deformed at steady state or that a given microstructure represents a steady state fabric, it is commonly assumed that these criteria must be at least approximately met in order to apply recrystallized grain size piezometry [e.g., *Christie and Ord*, 1980; *Kenkmann and Dresen*, 1998; *Stipp et al.*, 2010; *Trepmann and Stöckhert*, 2003; *Twiss*, 1977]. Certainly, as pointed out by *Trepmann and Stöckhert* [2003], a single stress value cannot be meaningfully applied to grains produced during a period of markedly fluctuating stress. *Twiss* [1977] predicted however that even at constant stress, a certain amount of strain or time is needed to achieve a microstructural steady state in which recrystallized grain size accurately reflects stress. Many of our high stress samples show imperceptible strains, <1% recrystallization by area, and were thus presumably quite far from steady state. Nevertheless, stress estimates based on small patches of recrystallized grains in these samples (e.g., Figure 2) are consistent with independent constraints. We suggest that, at least during bulge recrystallization of coarse-grained samples, the amount of time or strain needed (if any) for recrystallized grains to achieve a piezometrically appropriate size is too small to be of concern. This hypothesis is consistent with findings in coarse-grained nickel and other materials showing that recrystallized grain size is not a function of strain [*Humphreys and Hatherly*, 2004, pp. 432], and that equilibrium recrystallized grain size is already achieved in quartz deformed in laboratory experiments to a few percent strain [*Stipp et al.*, 2010, supplementary material]. (Although we note that the experiments referred to by *Stipp et al.* [2010] were not carried out in regime 1, perhaps the closest experimental analogue to Hsüehshan range deformation.) The wavelength of bulges along serrated grain boundaries is often at the same scale as recrystallized grains found elsewhere in samples (Figure 2) [e.g., *Platt and Behr*, 2011], thus it may be the case that even the very first recrystallized grains to form do so at a piezometrically-appropriate size. Experimental work on the evolution of recrystallized grain size in minerals is needed to better establish the conditions under which recrystallized grain size piezometry can reliably be carried out, and to link these conditions to indicative textural features.

6. Conclusions

[31] We estimate an integrated crustal strength in Taiwan of $\sim 1.7 \times 10^{12}$ N/m, with peak stress at the brittle-plastic transition ~200 MPa, and a coefficient of friction (μ) in the upper crust of 0.37. The consistency of these results with independent constraints indicates that the recrystallized grain size piezometer can be used to constrain stress histories in deformed rock with accuracy comparable to more widely used techniques, at least in relatively low-grade quartz. While we have only demonstrated consistency for one mineral under one set of conditions, similar grain size-stress relationships occur in other minerals (e.g., olivine, feldspar, calcite, ice, salt), offering potential for making accurate, small-scale observation of stress histories in a variety of geologic materials. We encourage further tests of paleopiezometry in quartz and other minerals under natural conditions, and envision eventual routine calibration and testing of numerical models using stress analyses of the rock record.

[32] **Acknowledgments.** We thank Whitney Behr, Timothy Byrne, Greg Hirth, John Suppe, Jian-Cheng Lee, and John Platt for input that helped clarify the ideas presented in this manuscript. Assistance in the field was provided by Chih-Tung Chen, Chung Huang, Aaron Martin, Yen-Chi Tseng, Shiao An-You, and Yong Chi-Kai. Reviewers Georg Dresen and Jan Tullis provided helpful feedback that improved the manuscript substantially. The Gordon and Betty Moore Foundation provided financial support. This is Caltech Tectonics Observatory contribution 200.

References

Austin, N. J., and B. Evans (2007), Paleowattmeters: A scaling relation for dynamically recrystallized grain size, *Geology*, *35*(4), 343–346, doi:10.1130/G23244A.1.

Austin, N. J., and B. Evans (2009), The kinetics of microstructural evolution during deformation of calcite, *J. Geophys. Res.*, *114*, B09402, doi:10.1029/2008JB006138.

Behr, W. M., and J. P. Platt (2011), A naturally constrained stress profile through the middle crust in an extensional terrane, *Earth Planet. Sci. Lett.*, *303*(3–4), 181–192, doi:10.1016/j.epsl.2010.11.044.

Beyssac, O., M. Simoes, J. P. Avouac, K. A. Farley, Y.-G. Chen, Y.-C. Chan, and B. Goffé (2007), Late Cenozoic metamorphic evolution and exhumation of Taiwan, *Tectonics*, *26*(6), TC6001, doi:10.1029/2006TC002064.

Bloomfield, J. P., and S. J. Covey-Crump (1993), Correlating mechanical data with microstructural observations in deformation experiments on synthetic two-phase aggregates, *J. Struct. Geol.*, *15*(8), 1007–1019, doi:10.1016/0191-8141(93)90173-8.

Bürgmann, R., and G. Dresen (2008), Rheology of the lower crust and upper mantle: Evidence from rock mechanics, geodesy, and field observations, *Annu. Rev. Earth Planet. Sci.*, *36*, 531–567, doi:10.1146/annurev.earth.36.031207.124326.

Burov, E. B., and A. B. Watts (2006), The long-term strength of continental lithosphere: "jelly sandwich" or "crème brûlée", *GSA Today*, *16*(1), 4–10, doi:10.1130/1052-5173(2006)016<4:TLTSOC>2.0.CO;2.

Byerlee, J. (1978), Friction of rocks, *Pure Appl. Geophys.*, *116*(4–5), 615–626, doi:10.1007/BF00876528.

Byrne, T., Y. C. Chan, R.-J. Rau, C. Y. Lu, Y.-H. Lee, and Y.-J. Wang (2011), The arc-continent collision in Taiwan, in *Arc-Continent Collision*, edited by D. Brown and P. D. Ryan, pp. 213–245, Springer, New York, doi:10.1007/978-3-540-88558-0_8.

Carena, S., J. Suppe, and H. Kao (2002), Active detachment of Taiwan illuminated by small earthquakes and its control of first-order topography, *Geology*, *30*(10), 935–938, doi:10.1130/0091-7613(2002)030<0935:ADOTIB>2.0.CO;2.

Chan, Y.-C., K. Okamoto, T.-F. Yui, Y. Iizuka, and H.-T. Chu (2005), Fossil fluid reservoir beneath a duplex fault structure within the Central Range of Taiwan: Implications for fluid leakage and lubrication during

earthquake rupturing process, *Terra Nova*, *17*(6), 493–499, doi:10.1111/j.1365-3121.2005.00636.x.

Chew, D. M. (2003), An Excel spreadsheet for finite strain analysis using the R-f/phi technique, *Comput. Geosci.*, *29*(6), 795–799, doi:10.1016/S0098-3004(03)00027-X.

Christie, J. M., and A. Ord (1980), Flow stress from microstructures of mylonites: Example and current assessment, *J. Geophys. Res.*, *85*(B11), 6253–6262, doi:10.1029/JB085iB11p06253.

Clark, M. B., D. M. Fisher, C.-Y. Lu, and C.-H. Chen (1993), Kinematic analyses of the Hsüehshan range, Taiwan: A large-scale pop-up structure, *Tectonics*, *12*(1), 205–217, doi:10.1029/92TC01711.

Dresen, G., J. Duyster, B. Stöckhert, R. Wirth, and G. Zulauf (1997), Quartz dislocation microstructure between 7000 m and 9100 m depth from the Continental Deep Drilling Program KTB, *J. Geophys. Res.*, *102*(B8), 18,443–18,452, doi:10.1029/96JB03394.

Dunlap, W., G. Hirth, and C. Teyssier (1997), Thermomechanical evolution of a ductile duplex, *Tectonics*, *16*(6), 983–1000, doi:10.1029/97TC00614.

Etheridge, M. A., and J. C. Wilkie (1981), An assessment of dynamically recrystallized grain-size as a paleopiezometer in quartz-bearing mylonite zones, *Tectonophysics*, *78*(1–4), 475–508, doi:10.1016/0040-1951(81)90025-1.

Exner, H. E. (1972), Analysis of grain- and particle-size distributions in metallic materials, *Int. Metall. Rev.*, *17*, 25–42, doi:10.1179/095066072790137729.

Fisher, D. M., C.-Y. Lu, and H. T. Chu (2002), Taiwan Slate Belt: Insights into the ductile interior of an arc-continent collision, in *Geology and Geophysics of an Arc-Continent Collision, Taiwan*, *Geol. Soc. Am.*, vol. 358, edited by T. Byrne and C. S. Liu, pp. 93–106, Geol. Soc. of Am., Boulder, Colorado, doi:10.1130/0-8137-2358-2.93.

Gourley, J. R., T. Byrne, Y.-C. Chan, F. Wu, and R.-J. Rau (2007), Fault geometries illuminated from seismicity in central Taiwan: Implications for crustal scale structural boundaries in the northern Central Range, *Tectonophysics*, *445*(3–4), 168–185, doi:10.1016/j.tecto.2007.08.013.

Grigull, S., S. M. Ellis, T. A. Little, M. P. Hill, and S. J. H. Buiter (2012), Rheological constraints on quartz derived from scaling relationships and numerical models of sheared brittle-ductile quartz veins, central Southern Alps, New Zealand, *J. Struct. Geol.*, *37*, 200–222, doi:10.1016/j.jsg.2012.01.006.

Hacker, B. R., A. Yin, J. M. Christie, and G. A. Davis (1992), Stress magnitude, strain rate, and rheology of extended middle continental-crust inferred from quartz grain sizes in the Whipple Mountains, California, *Tectonics*, *11*(1), 36–46, doi:10.1029/91TC01291.

Heilbronner, R., and J. Tullis (2002), The effect of static annealing on microstructures and crystallographic preferred orientation of quartzites experimentally deformed in axial compresion and shear, in *Deformation Mechanisms, Rheology and Tectonics*, *Geol. Soc. Spec. Publ.*, vol. 200, edited by S. De Meer et al., pp. 191–218, Tulsa, Okla., doi:10.1144/GSL.SP.2001.200.01.12.

Hirth, G., and J. Tullis (1992), Dislocation creep regimes in quartz aggregates, *J. Struct. Geol.*, *14*(2), 145–159, doi:10.1016/0191-8141(92)90053-Y.

Hirth, G., C. Teyssier, and W. Dunlap (2001), An evaluation of quartzite flow laws based on comparisons between experimentally and naturally deformed rocks, *Int. J. Earth Sci.*, *90*, 77–87, doi:10.1007/s005310000152.

Ho, C. S. (1988), *An Introduction to the Geology of Taiwan: Explanatory Text of the Geologic Map of Taiwan*, 2nd ed., 192 pp., Cent. Geol. Surv., Minist. of Econ. Affairs, Taipei, Taiwan.

Humphreys, F. J., and M. Hatherly (2004), *Recrystallization and Related Annealing Phenomena*, 2nd ed., 628 pp., Elsevier, Boston, Mass.

Jackson, J. (2002), Strength of the continental lithosphere: Time to abandon the jelly sandwich?, *GSA Today*, *12*(9), 4–10, doi:10.1130/1052-5173(2002)012<0004:SOTCLT>2.0.CO;2.

Kaus, B. J. P., C. Steedman, and T. W. Becker (2008), From passive continental margin to mountain belt: Insights from analytical and numerical models and application to Taiwan, *Phys. Earth Planet. Inter.*, *171*(1–4), 235–251, doi:10.1016/j.pepi.2008.06.015.

Kaus, B. J. P., Y. Liu, T. W. Becker, D. A. Yuen, and Y. Shi (2009), Lithospheric stress-states predicted from long-term tectonic models: Influence of rheology and possible application to Taiwan, *J. Asian Earth Sci.*, *36*(1), 119–134, doi:10.1016/j.jseaes.2009.04.004.

Kawabata, K., H. Tanaka, Y. Kitamura, and K.-F. Ma (2009), Apparent activation energy and rate-limiting process estimation from natural shale deformed by pressure solution in shallow subduction zone, *Earth Planet. Sci. Lett.*, *287*, 57–63, doi:10.1016/j.epsl.2009.07.032.

Kenis, I., J. L. Urai, W. D. Zee, C. Hilgers, and M. Sintubin (2005), Rheology of fine-grained siliciclastic rocks in the middle crust—evidence from structural and numerical analysis, *Earth Planet. Sci. Lett.*, *233*, 351–360, doi:10.1016/j.epsl.2005.02.007.

Kenkmann, T., and G. Dresen (1998), Stress gradients around porphyroclasts: Palaeopiezometric estimates and numerical modelling, *J. Struct. Geol.*, *20*(2–3), 163–173, doi:10.1016/S0191-8141(97)00074-6.

Kidder, S., J. P. Avouac, and Y. C. Chan (2012), Application of titanium-in-quartz thermobarometry to greenschist facies veins and recrystallized quartzites in the Hsüehshan range, Taiwan, *Solid Earth Discuss.*, *4*, 663–706, doi:10.5194/sed-4-663-2012.

Kim, K.-H., J.-M. Chiu, H. Kao, Q. Liu, and Y.-H. Yeh (2004), A preliminary study of crustal structures in Taiwan region using receiver function analysis, *Geophys. J. Int.*, *159*, 146–164, doi:10.1111/j.1365-246X.2004.02344.x.

Kohlstedt, D. L., B. Evans, and S. J. Mackwell (1995), Strength of the lithosphere–constraints imposed by laboratory experiments, *J. Geophys. Res.*, *100*(B9), 17,587–17,602, doi:10.1029/95JB01460.

Küster, M., and B. Stöckhert (1998), High differential stress and sublithostatic pore fluid pressure in the ductile regime—Microstructural evidence for short-term post-seismic creep in the Sesia Zone, Western Alps, *Tectonophysics*, *303*, 263–277.

Lacombe, O. (2001), Paleostress magnitudes associated with development of mountain belts: Insights from tectonic analyses of calcite twins in the Taiwan Foothills, *Tectonics*, *20*(6), 834–849, doi:10.1029/2001TC900019.

Lan, L. B., and P. J. Hudleston (1995), A method of estimating the stress exponent in the flow law for rocks using fold shape, *Pure Appl. Geophys.*, *145*(3–4), 621–635, doi:10.1007/BF00879592.

Lin, A. T., A. B. Watts, and S. P. Hesselbo (2003), Cenozoic stratigraphy and subsidence history of the South China Sea margin in the Taiwan region, *Basin Res.*, *15*, 453–478, doi:10.1046/j.1365-2117.2003.00215.x.

Lisle, R. J., H. E. Rondeel, D. Doorn, J. Brugge, and P. D. Gaag (1983), Estimation of viscosity contrast and finite strain from deformed elliptical inclusions, *J. Struct. Geol.*, *5*, 603–609, doi:10.1016/0191-8141(83)90072-X.

Liu, T. K., S. Hsieh, Y. G. Chen, and W. S. Chen (2001), Thermo-kinematic evolution of the Taiwan oblique-collision mountain belt as revealed by zircon fission track dating, *Earth Planet. Sci. Lett.*, *186*(1), 45–56, doi:10.1016/S0012-821X(01)00232-1.

Lu, C. Y. (1992), The development of the vein system in central Taiwan: a case study of the section from Kukua to Tekee along the Central Cross Island Highway, *J. Geol. Soc. China*, *35*(1), 77–94.

Ludwig, K. J. (2001), *Users Manual for Isoplot/Ex Rev. 2.49.*, *Berkeley Geochron. Cent. Spec. Publ.*, vol. 1a, 56 pp., Berkeley Geochron. Cent., Berkeley, Calif.

McIntosh, K., Y. Nakamura, T.-K. Wang, R. C. Shih, A. Chen, and C. S. Liu (2005), Crustal-scale seismic profiles across Taiwan and the western Philippine Sea, *Tectonophysics*, *401*, 23–54, doi:10.1016/j.tecto.2005.02.015.

Mercier, J.-C. C., D. A. Anderson, and N. L. Carter (1977), Stress in the lithosphere: Inferences from steady state flow of rocks, *Pure App. Geophys.*, *115*(1–2), 199–226, doi:10.1007/BF01637104.

Molnar, P., and H. Lyon-Caen (1988), Some simple physical aspects of the support, structure, and evolution of mountain belts, *Spec. Pap. Geol. Soc. Am.*, *218*, 179–207.

Mouthereau, F., and C. Petit (2003), Rheology and strength of the Eurasian continental lithosphere in the foreland of the Taiwan collision belt: Constraints from seismicity, flexure, and structural styles, *J. Geophys. Res.*, *108*(B11), 2512, doi:10.1029/2002JB002098.

Passchier, C. W., and R. A. J. Trouw (2005), *Microtectonics*, 2nd ed., Springer, Boston, Mass.

Paterson, M. S., and F. C. Luan (1990), Quartzite rheology under geological conditions, *Geol. Soc. Spec. Publ.*, *54*, 299–307.

Pitzer, K., and S. Sterner (1994), Equations of state valid continuously from zero to extreme pressures for H_2O and CO_2, *J. Chem. Phys.*, *101*, 3111–3116.

Platt, J. P., and W. M. Behr (2011), Grainsize evolution in ductile shear zones: Implications for strain localization and the strength of the lithosphere, *J. Struct. Geol.*, *33*(4), 537–550, doi:10.1016/j.jsg.2011.01.018.

Poirier, J. P. (1985), *Creep of Crystals: High-Temperature Deformation Processes in Metals, Ceramics, and Minerals*, 260 pp., Cambridge Univ. Press, New York, doi:10.1017/CBO9780511564451.

Ramsay, J. G. (1967), *Folding and Fracturing of Rocks*, 568 pp., McGraw Hill, New York.

Scholz, C. H. (2002), *The Mechanics of Earthquakes and Faulting*, Cambridge Univ. Press, New York, doi:10.1017/CBO9780511818516.

Sella, G. F., T. H. Dixon, and A. L. Mao (2002), REVEL: A model for recent plate velocities from space geodesy, *J. Geophys. Res.*, *107*(B4), 2081, doi:10.1029/2000JB000033.

Shih, R. C., C. H. Lin, H. L. Lai, Y. H. Yeh, B. S. Hwang, and H. Y. Yen (1998), Preliminary crustal structures across central Taiwan from

modeling of the onshore-offshore wideangle seismic data, *Terr. Atmos. Ocean. Sci.*, *9*, 317–328.

Shin, T. C. (1992), Some implications of Taiwan tectonic features from the data collected by the Central Weather Bureau Seismic Network [in Chinese], *Meteorol. Bull. Cent. Weather Bur.*, *38*, 23–48.

Simoes, M., and J. P. Avouac (2006), Investigating the kinematics of mountain building in Taiwan from the spatiotemporal evolution of the foreland basin and western foothills, *J. Geophys. Res.*, *111*, B10401, doi:10.1029/2005JB004209.

Simoes, M., J. P. Avouac, O. Beyssac, B. Goffé, K. A. Farley, and Y.-G. Chen (2007), Mountain building in Taiwan: A thermokinematic model, *J. Geophys. Res.*, *112*, B11405, doi:10.1029/2006JB004824.

Simoes, M., O. Beyssac, and Y.-G. Chen (2012), Late Cenozoic metamorphism and mountain building in Tawain: A review, *J. Asian Earth Sci.*, *46*(2), 92–119, doi:10.1016/j.jseaes.2011.11.009.

Stipp, M., and J. Tullis (2003), The recrystallized grain size piezometer for quartz, *Geophys. Res. Lett.*, *30*(21), 2088, doi:10.1029/2003GL018444.

Stipp, M., H. Stünitz, R. Heilbronner, and S. M. Schmid (2002), The eastern Tonale fault zone: a 'natural laboratory' for crystal plastic deformation of quartz over a temperature range from 250 to 700°C, *J. Struct. Geol.*, *24*, 1861–1884, doi:10.1016/S0191-8141(02)00035-4.

Stipp, M., J. Tullis, M. Scherwath, and J. H. Behrmann (2010), A new perspective on paleopiezometry: Dynamically recrystallized grain size distributions indicate mechanism changes, *Geology*, *38*(8), 759–762, doi:10.1130/G31162.1.

Stöckhert, B., M. R. Brix, R. Kleinschrodt, A. J. Hurford, and R. Wirth (1999), Thermochronometry and microstructures of quartz - a comparison with experimental flow laws and predictions on the temperature of the brittle-plastic transition, *J. Struct. Geol.*, *21*(3), 351–369, doi:10.1016/S0191-8141(98)00114-X.

Suppe, J. (2007), Absolute fault and crustal strength from wedge tapers, *Geology*, *35*(12), 1127–1130, doi:10.1130/G24053A.1.

Suppe, J., and J. H. Wittke (1977), Abnormal pore-fluid pressures in relation to stratigraphy and structure in the active fold-and-thrust belt of northwestern Taiwan, *Pet. Geol. Taiwan*, *14*, 11–24.

Thomas, J. B., E. B. Watson, F. S. Spear, P. T. Shemella, S. K. Nayak, and A. Lanzirotti (2010), TitaniQ under pressure: the effect of pressure and temperature on the solubility of Ti in quartz, *Contrib. Mineral. Petrol.*, *160*, 743–759, doi:10.1007/s00410-010-0505-3.

Tillman, K. S., and T. B. Byrne (1995), Kinematic analysis of the Taiwan Slate Belt, *Tectonics*, *14*(2), 322–341, doi:10.1029/94TC02451.

Tillman, K. S., T. B. Byrne, and C.-Y. Lu (1992), Pre-collision extensional structures from the central range, Taiwan: implications for the kinematic evolution of the South China Margin, *Acta Geol. Taiwan.*, *30*, 11–26.

Townend, J., and M. D. Zoback (2000), How faulting keeps the crust strong, *Geology*, *28*(5), 399–402, doi:10.1130/0091-7613(2000)28<399:HFKTCS>2.0.CO;2.

Treagus, S. H., and J. E. Treagus (2002), Studies of strain and rheology of conglomerates, *J. Struct. Geol.*, *24*, 1541–1567, doi:10.1016/S0191-8141(01)00162-6.

Trepmann, C. A., and B. Stöckhert (2003), Quartz microstructures developed during non-steady state plastic flow at rapidly decaying stress and strain rate, *J. Struct. Geol.*, *25*, 2035–2051, doi:10.1016/S0191-8141(03)00073-7.

Twiss, R. J. (1977), Theory and applicability of a recrystallized grain size paleopiezometer, *Pure Appl. Geophys.*, *115*, 227–244, doi:10.1007/BF01637105.

Ustaszewski, K., Y.-M. Wu, J. Suppe, H.-H. Huang, C.-H. Huang and S. Carena (2012), Crust-mantle boundaries in the Taiwan–Luzon arc-continent collision system determined from layered Vp models and local earthquake tomography, *Tectonophysics*, doi:10.1016/j.tecto.2011.12.029, in press.

van Daalen, M., R. Heilbronner, and K. Kunze (1999), Orientation analysis of localized shear deformation in quartz fibres at the brittle-ductile transition, *Tectonophysics*, *303*(1–4), 83–107, doi:10.1016/S0040-1951(98)00264-9.

Voll, G. (1976), Recrystallization of quartz, biotite and feldspars from Erstfeld to the Leventina nappe, Swiss Alps, and its geological significance, *Schweiz. Mineral. Petrogr. Mitt.*, *56*, 641–647.

Wightman, R., D. Prior, and T. Little (2006), Quartz veins deformed by diffusion creep-accommodated grain boundary sliding during a transient, high strain-rate event in the Southern Alps, New Zealand, *J. Struct. Geol.*, *28*(5), 902–918, doi:10.1016/j.jsg.2006.02.008.

Yamato, P., F. Mouthereau, and E. Burov (2009), Taiwan mountain building: insights from 2-D thermomechanical modelling of a rheologically stratified lithosphere, *Geophys. J. Int.*, *176*(1), 307–326, doi:10.1111/j.1365-246X.2008.03977.x.

Yen, T. P. (1973), The Eocene sandstones in the Hsüehshan range terrain, Northern Taiwan, *Proc. Geol. Soc. China*, *16*, 97–110.

Yue, L.-F. (2007), *Active Structural Growth in Central Taiwan in Relationship to Large Earthquakes and Pore-Fluid Pressures*, Princeton Univ., Princeton, N. J.

Zhou, D., H.-S. Yu, H.-H. Xu, X.-B. Shi, and Y.-W. Chou (2003), Modeling of thermo-rheological structure of lithosphere under the foreland basin and mountain belt of Taiwan, *Tectonophysics*, *374*(3–4), 115–134, doi:10.1016/S0040-1951(03)00236-1.